Improved detection of soma location and morphology in fluorescence microscopy images of neurons.

Cihan Bilge Kayasandik[a], Demetrio Labate[a,*]

[a]*Department of Mathematics, University of Houston, Houston, Texas 77204, United States of America*

Abstract

Background. Automated detection and segmentation of somas in fluorescent images of neurons is a major goal in quantitative studies of neuronal networks, including applications of high-content-screenings where it is required to quantify multiple morphological properties of neurons. Despite recent advances in image processing targeted to neurobiological applications, existing algorithms of soma detection are often unreliable, especially when processing fluorescence image stacks of neuronal cultures.
New Method. In this paper, we introduce an innovative algorithm for the detection and extraction of somas in fluorescent images of networks of cultured neurons where somas and other structures exist in the same fluorescent channel. Our method relies on a new geometrical descriptor called Directional Ratio and a collection of multiscale orientable filters to quantify the level of local isotropy in an image. To optimize the application of this approach, we introduce a new construction of multiscale anisotropic filters that is implemented by separable convolution.
Results. Extensive numerical experiments using 2D and 3D confocal images show that our automated algorithm reliably detects somas, accurately segments them, and separates contiguous ones.
Comparison with Existing Methods. We include a detailed comparison with state-of-the-art existing methods to demonstrate that our algorithm is extremely competitive in terms of accuracy, reliability and computational efficiency.
Conclusions. Our algorithm will facilitate the development of automated platforms for high content neuron image processing. A Matlab code is released open-source and freely available to the scientific community.

Keywords: Confocal microscopy, Fluorescence microscopy, Image analysis, Multiscale analysis, Neuronal morphology, Soma detection

1. Introduction

Structure-function relations are central to many questions concerning the study of biological systems. This is particularly true in the study of the central nervous system whose main functional units, the neurons, are highly specialized cells consisting of a cell body called *soma*, multiple tree-like processes called *dendrites* and a long thin process called *axon*. The remarkable morphological diversity of neurons found within and across brain regions shows the importance of structural characteristics for neuronal function.

Historically, the modern study of neuroanatomy can be traced back to the seminal work of Ramón y Cayal, around the end of 19th century. By adapting a staining technique discovered by Golgi in 1873, Cayal produced an impressive amount of highly detailed hand-drawn reconstructions of neuronal morphology. During the following century, in parallel with advances in microscopy and the development of more efficient and sensitive staining techniques, several methods were introduced to make neuronal reconstruction easier and more accurate, eventually replacing hand drawings with images generated via computer interface (see [1] for a detailed history). During the last two decades, several software toolkits were developed aiming at providing digital reconstruction of neurons from image acquired using bright field or fluorescent microscopy [2]. Even though most such methods require a significant component of manual intervention [3, 2] and algorithms tend to perform inconsistently with different types of data, a huge effort is still under way in the scientific community to create fully automated algorithms for problems of neuronal reconstruction. The impact of these methods in neuroscience is expect to be very significant. With respect to early manual reconstruction, digital reconstruction of neurons enables to quantify morphological properties in a way which was not previously possible. Results from digital reconstructions can be used to extract a multiplicity of morphometric measures, generate computational models, and carry out statistical analyses to investigate structural changes during development or induced by genetic or chemical perturbation.

The aim of this paper is to introduce a fully automated

*Corresponding author. Tel. +1 713 7433492; fax +1 713 7433505.
Email addresses: kayasa89@math.uh.edu (Cihan Bilge Kayasandik), dlabate@math.uh.edu (Demetrio Labate)

and computationally efficient algorithm for the accurate identification of soma location and morphology in fluorescence images of networks of neurons in culture. It is known that neuronal characteristics including soma volume and surface morphology are fundamental features for discriminating different types of neurons [4]. Detecting somas also plays a major role in extracting the connectivity and tree structure in a neuronal network as each soma location is identified with the root of a tree associated with the corresponding cell [5, 6].

In applications of high-content screening (HCS), multiple morphological properties of neurons need to be identified including soma location and shape characteristics. This information is usually collected from large sets of multi-channel fluorescence images so that automated processing methods are often necessary to handle such large data. However the automated analysis of confocal images of neuronal cultures presents a number of challenges. In cultures, somas are usually visible in the channel marked by the Microtubules Associated Protein 2 (MAP2) antibody staining or by a nucleus marker (e.g., DAPI or TROPO-3), neither of which is soma-selective. Hence further processing is needed to identify somas. An additional difficulty is that such confocal images typically consist of stacks containing 10-25 images. As a result, only 10-25 pixels are available along the z-direction as compared with the x and y directions which contain many more pixels (typically 512 or more). Due to this large difference in pixels number, it may be inefficient or even impossible to process such data using conventional 3D filters.

Automated or semi-automated methods for soma and cell detection found in standard image analysis packages frequently rely on binary masks generated by contrast enhancement and image intensity thresholding [7, 8]. While these methods can be very effective in phase-contrast microscopy [8, 9], they are often unreliable when applied to the analysis fluorescent images since high intensity values are commonly found outside somas. To deal with images where somas and other structures exist in the same fluorescence channel, a number of alternative methods proposed in recent years combine smoothing filters to regularize fluorescence intensity and classical morphological operators (e.g., morphological opening) to separate somas from connecting neurites [5, 10, 11, 12].

The main drawback of these methods is that they are very sensitive to the parameters of the algorithm so that they typically require a significant manual intervention to perform efficiently. In addition, many such methods have proven to be impractical or inefficient in the 3D setting, even though some recent studies have shown a clever way to process 3D information by projecting the original image stack onto its the three orthogonal planes [13].

To overcome the limitations of existing methods especially in the context of neuronal cultures, one of the authors introduced an innovative approach that relies on a novel multiscale descriptor called Directional ratio to separate somas from dendrites [14]. By quantifying the degree of local isotropy in images, this method was shown to detect somas very accurately and reliably in 2D images. However it is computationally intensive as it require the computation of multiple directional filters at various scales and the application of the level set algorithm. In addition, since more directions and larger filters are needed in 3D, the direct application of this method in 3D is impractical. One major aim of this paper is to introduce and demonstrate a major improvement of this method which relies on two novel ideas: (i) the application of a new class of multiscale directional filters which can be implemented by separable convolution to detect soma locations very efficiently; (ii) the application of the fast marching method to extract the soma regions and separate contiguous somas. Using these ideas we are able to speed up the extraction of somas in 2D image by over 20 times with respect to the results in [14] while keeping the same excellent level of accuracy and reliability. Remarkably, our method can detect somas even more efficiently than algorithms based on conventional morphological operators (known to be very fast) and much more accurately. Another contribution of this work is the algorithmic implementation of our new approach based on Directional Ratio to the 3D setting. The performance of our 2D and 3D algorithms is extensively validated on multiple confocal images of neuronal cultures and brain tissue, and successfully compared against state-of-the-art methods from the literature.

Our algorithms are implemented in Matlab and released open source under the GNU General Public Licence and freely available to the scientific community.

2. Materials and Methods

We consider the problem of detecting soma locations in fluorescent image stacks of neuronal cultures or neuronal tissue both in the 2D and 3D settings.

Our algorithm for soma detection and extraction – whether in 2D or 3D – consists of the following steps.

1. *Preprocessing.* It is designed to remove noise and improve image quality.
2. *Segmentation.* It separates neurons from background.
3. *Soma detection.* It is designed to find somas.
4. *Soma extraction.* It is designed to identify the entire soma regions and split somas that are clustered together.

In the following, we describe the methods we develop and apply to address each processing step, with most emphasis on the last two steps which contain our main original contributions.

2.1. Preprocessing

Preprocessing is designed to take full advantage of the capabilities of instrumentation by reducing sources of image degradation such as blurring and noise.

A common denoising routines found in biomedical applications is *Gaussian smoothing* [15], which consists in convolving an image with a Gaussian function $g(x) = \frac{1}{2\pi\sigma^2}\exp\left(-\frac{\|x\|^2}{2\sigma^2}\right)$, where σ^2 is a variance parameter. This operation has the effect of smoothing the image with a smoothing level controlled by σ^2. While this method is simple to implement and computationally efficient, it has the undesirable effect of blurring edges with the consequent loss of spatial information.

To avoid the above limitation, we adopt instead *wavelet shrinkage* which consists in: (i) transforming the image using the wavelet transform; (ii) filtering the resulting wavelet coefficients using a shrinkage function whose parameters are automatically determined from the data; (iii) applying the inverse wavelet transform to the shrinked coefficients to obtain a restored image. Wavelet shrinkage denoising was theoretically proven to be optimal with respect to the mean-squared error for estimating piecewise smooth signal corrupted by additive Gaussian noise [16, 17] and was shown to perform very competitively with fluorescence microscopy imaging data [18, 19, 20, 14].

2.2. Segmentation

A widely used image segmentation strategy is *intensity thresholding*, consisting in setting to 0 all pixels whose intensity value is below a certain threshold, and setting to 1 those pixels above or equal the threshold. To automatically set a threshold, a classical approach is Otsu's method [15], which assumes that the intensity distribution is bimodal and calculates the optimum threshold separating the two classes. The main downside of intensity thresholding is that it considers only the pixel intensity and ignores any relationships between pixels, with the result that pixels identified in the region of interest may fail to be contiguous. This performance issue is more severe as the noise level increases.

To ensure a more faithful preservation the geometry of data, we adopt in this paper a segmentation strategy based on Support Vector Machines (SVM) originally introduced by one of the authors [21, 22] and whose main novelty is the use of features generated by a set of multiscale Laplacian and multiscale directional filters designed to capture tubular structures in neuronal images. As for many algorithms of this type, the proper classification stage of the algorithm is preceded by a training stage of the classifier which may be computationally intensive. For the training stage, we selected 2 images out of 20, containing a total of 11 neurons (out of 71 neurons in the 20 images). Feature vectors were generated using 10 filters comprising Laplacian and directional filters at multiple scales. We remark that the training stage needs to be run only once as long as the segmentation algorithm is applied to images of the same type (e.g., same cell type and image acquisition setting). Fig. 1 illustrates the segmentation of a 2D image of a neuronal culture using different strategies. The result reported in the figure suggests that the SVM approach is more effective at capturing the true data structure.

2.3. Soma detection

Our method for soma detection relies on the Directional Ratio, an approach recently introduced by one of authors to quantify the degree of local isotropy in an image [18, 23] and shown to be very effective for separating somas from neurites in fluorescent images of neurons [14].

2.3.1. Directional Ratio

Given a collection of multiscale orientable filters $\{\phi_{j,\ell}\}$, where the indices j, ℓ are associated with a range of scales and orientations, respectively, the *Directional Ratio* of an image f at the j-th scale and at location p is the quantity

$$D_j f(p) = \frac{\min_\ell\{|f * \phi_{j,\ell}(p)|\}}{\max_\ell\{|f * \phi_{j,\ell}(p)|\}}\,. \tag{1}$$

For instance, in dimension 2, the simplest choice of filters $\phi_{j,\ell}$ are the functions

$$\phi_{j,\ell}(x) = \chi_{S_{j,\ell}}(x),$$

where χ_A is the indicator function of A and the sets $S_{j,\ell}$ are the scaled and rotated rectangles $S_{j,\ell} = 2^j R_{\theta_\ell} S$, where $R_\theta = \begin{pmatrix} \cos\theta & \sin\theta \\ -\sin\theta & \cos\theta \end{pmatrix}$ and S is a fixed rectangle. Clearly, the same idea applies in the 3D setting if one replaces 2D rectangles with 3D rectangles and uses 3D rotations.

The Directional Ratio ranges between 0 and 1, and it measures the degree of directional coherence of an image f at given scale and location. It is proved in [18, 23] that, if f is an image containing blob-like and vessel-like structures, then, for an appropriate range of scales controlled by j, there exists a threshold T significantly less than 1 such that the Directional Ratio does not exceed T when p is located inside a vessel-like structure; by contrast, when p is located strictly inside a blob-like structures then the Directional Ratio is close to 1 (See Fig. 2). Note that the Directional Ratio is not guaranteed to be close to 1 near the boundary of a blob-like structure. Nevertheless it was shown that one can reliably detect somas in a segmented image of a neuron f by computing the Directional Ratio $D_j f(p)$ at an appropriate scale controlled by j and discarding those points p for which $D_j f(p) < T$. Specifically, j is chosen so that the filter length is larger than the radius of the neurites and close to the radius of the somas.

The practical implementation of (1) requires computing multiple filtered images $f * \phi_{j,\ell}$ for various orientations ℓ (at a fixed scale j). For a 2D image f of size $N \times N$ the computation of each filtering step $f * \phi_{j,\ell}$ using FFT to implement convolution requires $O(N^2 \log N)$ operations. Using L orientations, this brings the total number of operations to $O(LN^2 \log N)$. Applying the same reasoning in 3D, with the same density of orientations, the computational cost would be $O(L^2 N^3 \log N)$ operations. This shows that the computational cost of directly implementing (1), as it was carried out in [14], is already significant in 2D and would be unacceptable in the 3D setting. A test

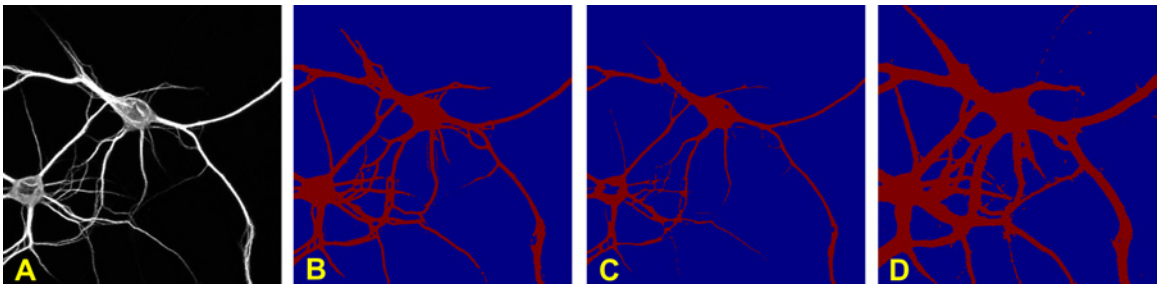

Figure 1: **Comparison of segmentation routines.** (A): Denoised image of a neuronal culture. (B-D): Image segmentation results using our SVM-based method (B); intensity thresholding, Otsu's method (C); intensity thresholding, threshold based on median of the image (D).

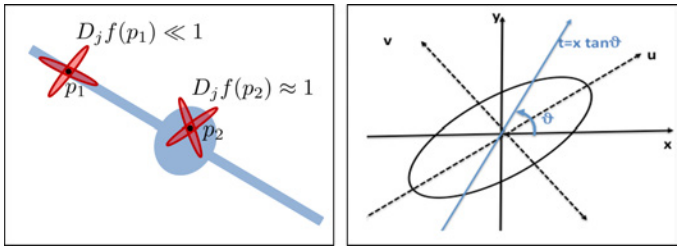

Figure 2: **Directional Ratio and directional filters.** Left: Due to the different behavior of orientable filters, for an appropriate range of scales, the Directional Ratio is much smaller than 1 at p_1 inside a vessel, and it is about 1 at p_2, inside a blob structure. Right: A rotated anisotropic Gaussian can be decomposed along its main axes u and v or alternatively along the non-orthogonal axes x and t. The second choice enables fast implementation by separable convolution.

on a $512 \times 512 \times 512$ image stack run on a standard laptop (2.4GHz processor) with a Matlab code requires about 103 hours to compute the Directional Ratio with $L^2 = 40$ directional filters. In this paper, we develop a new construction and implementation of directional filters based on multiscale orientable filters implemented by separable convolutions. Using this new approach, we can significantly reduce the computational cost both in the 2D and 3D settings. As shown in the Results section below, using the same laptop we can process the same 3D stack in about 1 minute.

2.3.2. Anisotropic Gaussian filters

Several constructions of orientable anisotropic filters were proposed in the literature such as the classical rotated Gaussians by Perona [24] and the shearlet filters [25, 26]. Many such constructions aim at providing additional properties, e.g., shearlet filters are particularly sensitive to edges. For our application to the computation of the Directional Ratio (1), our requirements are very mild as we only need orientable waveforms with anisotropic support. Since we are mostly concerned with reducing the computational cost of the Directional Ratio, in this paper we will focus on a class of anisotropic Gaussian filters that can be implemented and computed very efficiently.

In 2 dimensions, an anisotropic Gaussian function is obtained by scaling a 2D Gaussian using different factors σ_x and σ_y (say, $\sigma_x = 10\sigma_y$) in the x and y directions, respectively:

$$g_0(x, y; \sigma_x, \sigma_y) = \frac{1}{2\pi\sigma_x\sigma_y} \exp\left(-\frac{1}{2}\left(\frac{x^2}{2\sigma_x^2} + \frac{y^2}{2\sigma_y^2}\right)\right).$$

By rotating the coordinate axes by an angle θ, one obtains the oriented anisotropic Gaussian functions

$$g_\theta(x, y; \sigma_x, \sigma_y) = \frac{1}{2\pi\sigma_x\sigma_y} \exp\left(-\frac{1}{2}\left(\frac{(x\cos\theta + y\sin\theta)^2}{\sigma_x^2} + \frac{(-x\sin\theta + y\cos\theta)^2}{\sigma_y^2}\right)\right).$$

Geusebroek et al [27] introduced a very efficient method to separate the convolution with the anisotropic Gaussian $g_\theta(x, y; \sigma_x, \sigma_y)$ as the composition of a 1D convolution with a Gaussian filter in the x direction followed by another 1D convolution with a Gaussian filter in a non-orthogonal direction, that is

$$g_\theta(x, y; \sigma_x, \sigma_y) = \frac{1}{2\pi\sigma_x\sigma_\phi} \exp\left(-\frac{1}{2}\frac{x^2}{\sigma_x^2}\right) * \exp\left(-\frac{1}{2}\frac{t^2}{\sigma_\phi^2}\right),$$

where $t = x\cos\phi + y\sin\phi$ and ϕ is an appropriate functions of θ. An illustration of this decomposition is shown in Fig. 2. Using a recursive approximation to implement 1D Gaussian convolutions, this method yields an implementation that is very accurate and faster than a FFT-based 2D convolution, as it requires only $O(1)$ multiplications per pixel. We adopt this implementation to compute our Directional Ratio. In this case, the scale of the filters is controlled by σ_x and σ_y.

The same idea extends to the n-dimensional case, as shown by Lampert and Wirjadi [28]. In particular, similar to the 2D case we can represent any 3-dimensional rotated anisotropic Gaussian filters as the composition of 3 1-dimensional Gaussian filters aligned along non-orthogonal directions. Again these filters have fast implemention using separable convolution.

2.4. Soma extraction

As we observed above, the Directional Ratio of the segmented image of a neuron is expected to be close to 1 inside a soma but its value may be much lower near its

boundary. Hence, by thresholding the Directional Ratio, we will only find a region strictly inside the soma (see Fig. 3). To identify the entire soma including the region near its boundary, we need to grow the initial soma region. In this paper we develop an approach based on the Fast Marching method.

2.5. Level Set and Fast Marching methods

The *Level Set* and *Fast Marching* methods are variational approaches introduced to track evolution of curves and shapes without having to parametrize these objects [29, 30]. In [14], we used the Level Set approach with the boundary curve of the region found by the Directional Ratio inside the soma as the initialization curve Γ of the level set evolution equation. Even though this method provides excellent results, it is computationally intensive and its direct extension to the 3D setting is impractical.

As an alternative faster approach for tracking a moving boundary, we apply here the Fast Marching method which is designed for problems in which the speed function never changes sign, so that the front is always moving forward or backward. This assumption allows one to convert the evolution problem to a stationary formulation, which has much faster implementation (about $N \log N$ operations for an N size grid) than Level Set method, even though the latter one is more flexible.

Fast marching method builds the evolving curve Γ by computing the arrival time $T(p)$, as the time when the curve crosses a location p, by using a speed map F given by the user. The selection of F is the critical factor in the application of this method.

In our situation, taking again the boundary curve of the initial soma region as the initialization curve, we want the speed map F of the evolving curve to decrease as it approaches the boundary of the soma and to finally stop at the boundary. This suggests that the Directional Ratio of the segmented image could be a good candidate for the velocity map as its values are larger inside the soma and decrease at the boundary. However, the Directional Ratio does not vanish near the boundary of the soma and at the connected neurites, so that the curve Γ would continue to evolve outside the soma and inside the neurites. To deal with this problem, we use the following strategy. To generate a sharper decrease away from the interior of the soma, we set $F(p)$ equal to the modified Directional Ratio

$$\frac{\min_\ell\{|f * \phi_{j,\ell}(p)|^3\}}{\max_\ell\{|f * \phi_{j,\ell}(p)|\}}.$$

Due to the power introduced in the numerator, this quantity decreases faster than the Directional Ratio away from the soma. Additionally, this function is thresholded by setting to 0 very small values (below 0.00001 in our experiments) to ensure that the evolution will stop when Γ reaches the soma's boundary.

For our numerical implementation of the Fast Marching method, we adapted the Fast Marching Matlab toolbox by G. Peyré which is based on [31, 30].

2.5.1. Separation of clustered somas

Our method to extract somas may detect multiple contiguous somas as a single one. To address this issue, we use the following approach developed by one of the authors in [14]. After applying our method based on Directional Ratio at the default scale, we check the extracted soma area. If this area differs from the expected area more than three times the estimated standard deviation, then we conclude that it contains more than one soma. Next, we compute again the Directional Ratio at a coarser scale, that is, using twice as long directional filters; the application of a threshold on the Directional Ratio will now produce a smaller initial set inside each true soma region. Finally, we apply again the Fast Marching routine using the new boundary curves for each initial set. This method is run automatically and, as shown by numerical tests in the Results section, reliably separates contiguous somas.

2.6. Specimen preparation and imaging

Images used in this paper are primary hippocampal neuronal cultures that were prepared in Dr. Laezza's Laboratory at the Department of Pharmacology & Toxicology of the University of Texas Medical Branch.

Confocal images were acquired with a Zeiss LSM-510 Meta confocal microscope with either a 63X or a 40X oil immersion objective (1.4 NA). Multi-track acquisition was done with excitation lines at 488 nm for Alexa 488, 543 nm for Alexa 568 and 633 nm for Alexa 647. Respective emission filters were band-pass 505-530 nm, band-pass 560-615 nm and low-pass 650. Stacks were collected at z-steps of 1 μm with a frame size of 512 $\times$ 512, pixel time of 2.51 μs, pixel size 0.28 $\times$ 0.28 μm (63X objective) or 0.44 $\times$ 0.44 μm (40X objective) and a 4-frame Kallman averaging.

Banker's style hippocampal neuron cultures were prepared from embryonic day 18 (E18) rat embryos as described in [32]. Briefly, following trituration through a Pasteur pipette, neurons were plated at low density (105 $\times$ 105 cells/dish) on poly-L-lysine-coated coverslips in 60 mm culture dishes in MEM supplemented with 10% horse serum. After 24 h, coverslips (containing neurons) were inverted and placed over a glial feeder layer in serum-free MEM with 0.1% ovalbumin and 1 mM pyruvate (N2.1 media; Invitrogen, Carlsbad, CA) separated by approx. 1 mm wax dot spacers. To prevent the overgrowth of the glia, cultures were treated with cytosine arabinoside at day 3 in vitro (DIV).

Hippocampal neurons (DIV14) were fixed in fresh 4% paraformaldehyde and 4% sucrose in phosphate-buffered saline (PBS) for 15 min. Following permeabilization with 0.25% Triton X-100 and blocking with 10% BSA for 30 min at 37 °C, neurons were incubated overnight at room temperature with the following primary antibodies: mouse anti-FGF14 (monoclonal 1:100; Sigma Aldrich, St Louis, MO), rabbit anti-PanNav (1:100; Sigma, St Louis, MO) and chicken anti-MAP2 (polyclonal 1:25000; Covance, Princeton, NJ) diluted in PBS containing 3% BSA. Neurons were

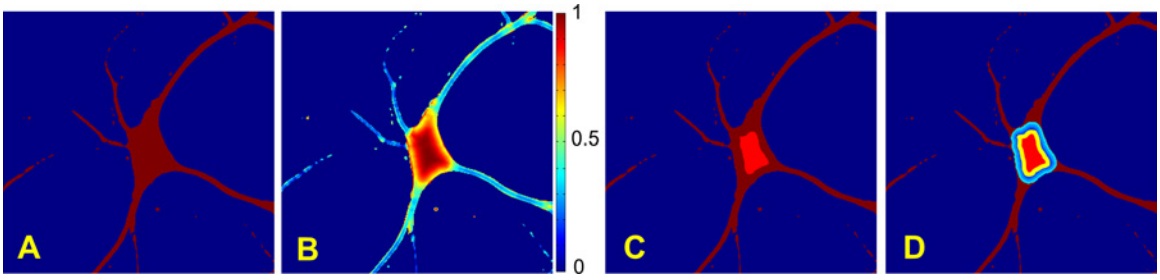

Figure 3: **Soma extraction.** Starting from the segmented image of a neuron (A), we compute the Directional Ratio in (B); whose values range from 0 (blue) to 1 (red). By thresholding those pixels in (B) was value in above 0.85, we detect an initial soma region in (C). We apply the Fast Marching algorithm to evolve the boundary of the initial soma region in (C) until it finds the entire soma region in (D).

then washed 3 times in PBS and incubated for 45 min at 37 °C with appropriate secondary antibodies as described for brain tissue staining. Coverslips were then washed 6 times with PBS and mounted on glass slides with Prolong Gold anti-fade reagent.

All the animal procedures were performed in accordance to the University of Texas Medical Branch at Galveston IACUC approved protocols.

3. Results and Discussion

In this section, we illustrate the application of our improved soma detection and extraction algorithm on multiple fluorescent images of neurons both in the 2D and 3D settings. Imaging data, as indicated above, were provided by Dr. Laezza at the Department of Pharmacology & Toxicology of the University of Texas Medical Branch. Our numerical code is written in Matlab and includes the routine for the computation of anisotropic Gaussian filters and Fast Marching propagation described above. All numerical experiments were run using a MacBook with Intel Core i5 2.4GHz processor and 16 GB RAM. Data and open source code used to generate our results are publicly available at `https://github.com/cihanbilge/SomaExtraction`.

3.1. Performance metric

To assess the performance of our algorithm on soma extraction, we adopt the following standard statistical measures of the performance of a binary classification test [33]. The *True Positive Rate TPR* (or *Sensitivity*) measures the proportion of correctly identified soma pixels with respect to the total number of true soma pixels, which are manually identified by a domain-expert (without knowledge of the algorithm results). Denoting by TP (= true positive) the number of correctly identified soma pixels and by FN (= false negative) the number of true soma pixels incorrectly rejected, we define:

$$TPR = \frac{TP}{TP + FN}.$$

The *False Positive Rate FPR* (this is the complement of the *Specificity*) measures the proportion of pixels incorrectly identified as soma pixels with respect to the total number of true soma pixels. That is, denoting by FP (= false positive) the pixels incorrectly selected as soma pixels, we define

$$FPR = \frac{FP}{TP + FN}.$$

This rate is a penalty akin to wrong soma pixel detections. When our FPR is compared with the traditional definition $(FP)/(TN + FP)$, one notices that this last expression would be very close to zero in our neuronal images since false soma detections are much less than the number of background pixels, due to the low neuronal density in our images. Hence, we adopted a new modified definition which describes false soma detections as a percentage of soma volume measured in pixels. Finally, the *Dice Coefficient* DC is used to compare the similarity between two samples or measures and is given by

$$DC = \frac{2\,TP}{2\,TP + FN + FP}.$$

Note that the denominator $2\,TP + FN + FP = TP + FP + FN + TP$ is the sum of the detected pixels and the true soma pixels. DC can be considered as a measure of the overall effectiveness of the soma extraction algorithm.

3.2. 2D soma analysis

Due to the difficulty of processing an image stack in 3D resolution, in several studies stacks are converted into 2D images by computing projections along the axis perpendicular to the image plane (the z axis). The *maximum intensity projection* (MIP) for instance maps an image stack into a 2D image where each pixel contains the maximum value over all images in the stack at that pixel location.

For our 2-dimensional tests, we considered 20 MIP images obtained from 20 standard field-of-view confocal image stacks of low-density neuronal cultures, as commonly used in phenotypic screenings of analytes for drug-discovery or biomarker identification (cf. [34, 35, 36, 32]). Each image stack comprises between 10 and 25 images and contains between 1 and 10 neurons, for a total of 71 somas in the 20 data sets we considered. According to the processing pipeline described in the Materials and Methods section, images were first preprocessed and segmented; the Directional Ratio was computed; an initial

region was obtained by thresholding the Directional Ratio with threshold = 0.85; finally, by applying the Fast Marching algorithm to the initial region, somas were extracted and contiguous somas separated, if needed.

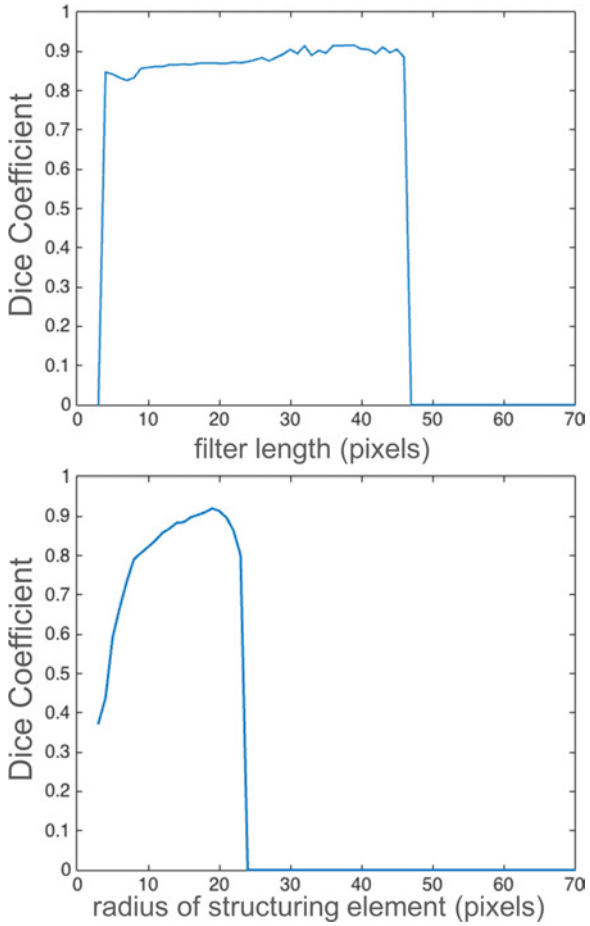

Figure 4: **Sensitivity on scale parameter.** Plots illustrate the soma extraction performance, according to the Dice Coefficient, as a function of the filter length for our algorithm (above) and as a function of the radius of the structuring element for an algorithm using the morphological opening operator (below).

For the implementation of the Directional Ratio, we considered the two types of directional filters described above, i.e., rectangular and anisotropic Gaussian filters. As this method requires filtering an image at multiple orientations and at appropriate scale, we need to select the scale parameter and the number of orientations.

According to the theory, the scale parameter must be selected such that filter length is close to the radius of the somas, say 85% of it. Our data include images acquired at magnification 40X and 63X, and on such data the expected radius of a soma is about 32 and 48 pixels, respectively. This estimate is based on randomly selecting 5 somas in each set of images and averaging the diameters measured on the images.

Hence, setting the filter length L of our rectangular filters to 85% of the estimated soma radius, we have $L = 27$ and $L = 40$ pixels for our two types of images, respectively. Similarly, for the anisotropic Gaussian filters, we set σ_x equal to 9 and 13 pixels, respectively (here we assume that the length of the filter is approximately $3\sigma_x$). Fig. 4 shows that the performance of our algorithm is clearly dependent on the selection of the scale parameter but not too sensitive to its value. Even though, for the image considered here, our method performs better when filter length is near 40 pixels, yet the algorithm performance is overall very consistent in the range 5-45 pixels. By contrast, the figure shows that a method based on conventional morphological operators is typically much more sensitive to the scale parameter.

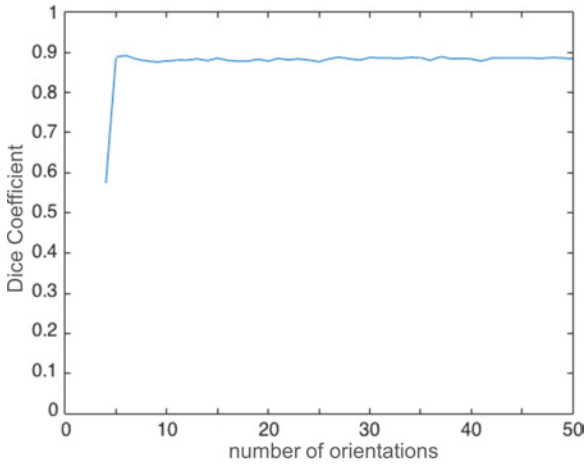

Figure 5: **Sensitivity on the number of orientations.** The plot illustrates the sensitivity of our algorithm performance, according to the Dice Coefficient, as a function of the number of orientations of the directional filters.

For the selection of the number of orientations, it is expected that the algorithm performance would improve (or at least would not worsen) by increasing the number of orientations since the Directional Ratio would become potentially more able to detect changes in geometry. On the other hand, computing time increases with the number of orientations as more filtered images are being computed; thus, we wish to keep this number relatively low. The analysis of the sensitivity of the algorithm as a function of this parameter, as illustrated in Fig 5, shows that the performance of the algorithm stabilizes very rapidly when the number of orientations increases and there is essentially no performance improvement choosing more than 7 or 8 orientations. Therefore, in all our experiments we selected 10 uniformly spaced orientations.

Figure 6 illustrates the application of our algorithm using anisotropic Gaussian filters (with default parameters $\sigma_x = 9$ and 10 orientations) on a representative MIP image of a neuronal culture of size 512×512 pixels containing five somas. The figure shows that the algorithm correctly detects somas and separates contiguous ones.

To benchmark the performance of our algorithm, we applied it to our 20 images and compared it against multiple state-of-the-art algorithms. For the comparison, we considered: the method based on Directional Ratio and

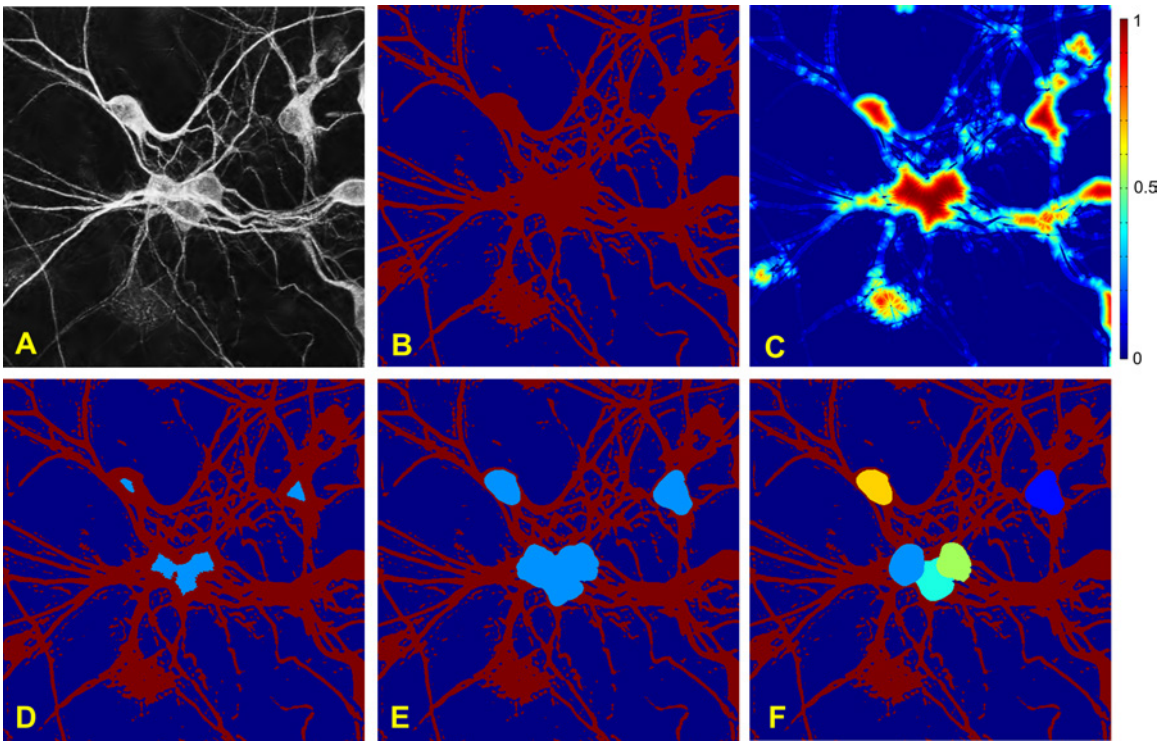

Figure 6: **2D soma detection and extraction.** (**A**) Denoised image obtained using a wavelet-based routine on the MIP of the image stack. Image size = 512×512 pixels (1 pixel = $0.28 \times 0.28 \mu m$). (**B**) Segmented binary image from SVM based segmentation. (**C**) Directional ratio plot; values range between 1, in red color (most isotropic regions), and 0, in blue color (least isotropc regions); the Directional Ratio is only computed inside the segmented region, i.e., the red region in Panel B. Anisotropic Gaussian filters are used for directional filtering. (**D**) Detection of initial soma region obtained by thresholding values below 0.85 in Panel C. (**E**) Soma segmentation obtained by applying the fast marching method with the initialization curve determined by the boundary of the initial soma region in Panel D. (**F**) Separation of contiguous somas.

level set by Ozcan et al. [14], henceforth denoted as DR-Lev; the algorithms based on conventional morphological operator by Vallotton et al. [11] and by Schmitz et al. [12], henceforth denoted as Morph1 and Morph2, respectively. For our algorithm, we consider two variants where the directional filters are rectangular or anisotropic Gaussian functions; henceforth we refer to these two versions of the algorithm as DR-Rec and DR-Gau, respectively. For Morph1 and Morph2, we need to set the value of the radius of the structuring element associated with the morphological opening operator. Based on the indication from the original papers, for two types of images considered in our tests, we set this value to 15 and 23 pixels, respectively. For DR-Rec, DR-Gau, DR-Lev, we used default scale parameter and number of orientations, as described above.

The performance of our algorithm and its baseline comparison with the various competing methods is reported in Table 1. The table lists the soma detection rate in terms of True Positive (TP), False Positive (FP) and False Negative(FN), the performance metrics FPR, TPR and DC for soma extraction, and the computing times for soma detection and extraction. The table shows that methods based on Directional Ratio provide overall very competitive performance for both soma detection and extraction. They have perfect or excellent detection rate and best extraction performance. By contrast, the soma detection and extraction performance of Morph1 and Morph2 is significantly lower; Morph2 performs better than Morph1. Concerning computing time, DR-Gau has the fastest computing time for soma detection, thanks to the implementation of directional filters by separable convolution; computing time is about 4 times longer for all other methods, including DR-Rec, where filtering is implemented by regular 2D convolution. As Morph1 and Morph2 have no separate routines for detection and extraction, the reported computing times are the same. These methods exhibit the fastest computing time for extraction. Among methods based on Directional Ratio, DR-Gau is the fastest one, whereas Dr-Lev is about 40 times slower. As argued in the Materials and Methods section, this difference is due mostly to the significant difference in computational cost between the Level Set and Fast Marching routines. Results in the table show that, despite the huge difference in computing time, the use of either one of the two routines has negligible impact on soma extraction performance hence it is a major advantage to use the Fast Marching method in this algorithm.

The performance of each algorithm presented above depends on the combined performances of their segmentation and soma extraction subroutines. As observed in the Ma-

Table 1: **Performance Comparison.** Performance analysis of different soma detection and extraction algorithms using 20 images containing 71 somas in total. TP=true positive, FP=false positive, FN=false negative, TPR=true positive rate, FPR=false positive rate, DC=dice coefficient.

	DR-Gau	DR-Rec	Morph1	Morph2	DR-Lev
Soma detection rate: correct, misidentified, missed (TP, FP, FN)	100%, 0%, 0% (71, 0, 0)	100%, 0%, 0% (71, 0, 0)	76%, 10%, 24% (54, 6, 17)	96%, 19% , 3% (69, 16, 2)	99%, 0% , 1% (70, 0, 1)
TPR (soma extraction)	0.95	0.99	0.83	0.95	0.95
FPR (soma extraction)	0.28	0.40	1.72	1.15	0.23
DC (soma extraction)	0.86	0.84	0.52	0.77	0.87
Comp. time: detect	0.21 s	0.86 s	0.90 s	0.90 s	0.86 s
Comp. time: detect+extract	4.01 s	4.45 s	0.90 s	0.90 s	157.76 s

terials and Methods section, intensity thresholding is not expected to perform as effectively as our SVM-based segmentation routine but the former method is significantly faster than the other one. Similarly, conventional morphological operators as those used in Morph2 to extract somas are faster than our method combining Directional Ratio and Fast Marching routine. To better illustrate the impact of each subroutine, we report in Table 2 the values of detection rate, DC and computing time obtained from various combinations of segmentation (SVM = SVM-based segmentation; Thr = intensity thresholding segmentation as in MORPH2) and soma extraction subroutines (DR = Directional Ratio and Fast Marching; Morph = morphological opening operator as in MORPH2).

Table 2: **Analysis of computational cost.** Computational cost and performance of different combinations of image segmentation and soma extraction routines, using 20 images (total somas=71).

	SVM + DR	SVM + Morp	Thr + DR	Thr + Morp
Detect. rate: correct, misidentified, missed (TP, FP, FN)	100% 0%, 0% (71, 0, 0)	96% 8%, 3% (69, 6, 2)	94% 0%, 6% (67, 0, 4)	96% 19% , 3% (69, 16, 2)
DC (extraction)	0.86	0.77	0.81	0.77
Comp. time	8.21 s	8.9 s	0.91 s	1.6 s

The table shows that our Directional Ratio routine for soma extraction consistently improves the algorithm performance. If the segmentation routine is implemented using our SVM-based segmentation, then a better DC value (the best overall) and a faster computing time is achieved using Directional Ratio rather than morphological opening operator. Similarly, if the segmentation routine is implemented using the morphological opening operator, again a better DC value and a faster computing time (the best overall) is achieved using the Directional Ratio.

Another observation is that the SVM-based segmentation routine has the largest impact in the overall computing time of the algorithm. By replacing this routine with a method based on intensity thresholding, the total computing time decreases from 8.21 to 0.91 s. However, this comes with a significant downgrade in performance as DC decreases from 0.86 to 0.81 and the detection rate worsens (4 somas are missed). This observation is consistent with the segmentation result shown in Fig 1 using a representative MIP image of a neuronal culture. The figure shows that the segmentation result based on intensity thresholding may miss regions inside a soma or produce over-segmented images leading to false positive or false positives, as in fact is observed in Table 1.

3.2.1. Automated scale selection

As noticed above, the application of our algorithm for soma detection requires setting the length of the filter based on the radius of the soma. In our experiments above, this quantity was estimated from a statistical analysis of the data and it could be predicted based on the type of neurons and magnification setting of the microscope.

Alternatively, to estimate the radius of somas in an image without any external input from the user, one could try to apply classical scale-space analysis [37] to automatically select the image scale. However, due to the irregularity of soma shapes and the common occurrence of thick neurites, we found that the direct application of this method to our images is very unreliable, as it will frequently misidentify somas (at locations inside thick neurites) and significantly underestimate or overestimate their radius (due to their irregular shapes). To avoid such shortcomings, we developed a modified approach to carry over scale-space analysis using the family of anisotropic multiscale filters we introduced above. Our scale selection algorithm is applied to a segmented image and includes the following steps: (1) the segmented image is filtered using anisotropic Gaussian filters at 2 orthogonal directions for a range of scales (e.g., $\sigma_x = 1$ to 20 pixels with 1 pixel increment); (2) locations of local maxima of the filtered image as a function of the scale are detected, for the two filtered directions; (3) the soma radius is estimated, for each detected local maximum location, as the smaller of the two scales detected. We found that this simple method is fast to compute as it relies on filters that are implemented by separable convolution (computing time is 0.67 s on one of our 512×512 images) and performs rather well. Results reported in Table 3 show that the DC value computed on our set of images using DR-Gaus with automated scale selection is slightly lower than the one found above (DC=0.84 vs. DC=0.86). For comparison, we also included the performance results using Morph2 showing that also in this case we find a lower

DC value (DC=0.69 vs. DC=0.77). In fact, as expected due to the higher sensitivity of Morph2 to scale selection, the performance decrease is more significant in this case.

Table 3: **Performance Comparison with automated scale selection.** Performance analysis of different soma detection and extraction algorithms using 20 images containing 71 somas in total. DR-Gau-asl = DR-Gau with automated scale selection; Morph2-asl= Morph2 with automated scale selection.

	DR-Gau-asl	DR-Gau	Morph2-asl	Morph2
Detect. rate: correct	100%	100%	92%	96%
misidentified, missed	0%, 0%	0%, 0%	8%, 28%	19% , 3%
(TP, FP, FN)	(71, 0, 0)	(71, 0, 0)	(65, 6, 20)	(69, 16, 2)
TPR (soma extraction)	0.90	0.95	0.86	0.95
FPR (soma extraction)	0.29	0.28	1.16	1.15
DC (soma extraction)	0.84	0.86	0.69	0.77

The lower perfomance found using automated scale selection is due to the difficulty in estimating correctly soma radii. For instance, the presence of contiguous somas is not recognized by our algorithm and introduces significant errors. Addressing this and other limitations of the scale selection algorithm is however beyond the scope of this paper.

3.3. 3D soma analysis

We tested our 3D algorithm for soma detection and extraction on two sets containing different types of imaging data: Set1 consists of 3 confocal image stacks of brain tissue, each stack containing 1-2 somas; Set2 consists of 3 confocal image stacks of neural cultures, each stack containing 7-8 somas.

Computational cost is a major issue for the analysis of 3D data due to the impact of 3D filtering. As discussed above, the application of our method based on Directional Ratio to the analysis of 3D data using conventional 3D filters would be highly impractical; on an image of size $512 \times 512 \times 512$, using 40 orientations, it would take over 100 hours. Therefore, in our tests of our algorithm, we only considered anisotropic Gaussian directional filters which are implemented via separable convolution and not rectangular filters. We used 40 orientations for our experiments.

Fig. 7 illustrates the application of our algorithm for 3D soma extraction on representative image stacks.

To assess the performance of our approach, we employed the same metrics we adopted in the 2D setting. As baseline comparison, we implemented a 3D extension of the method based on the morphological opening operator proposed by [12] (the method is only applied in 2D in the original paper). To adapt the method to the different geometry of the dataset, for the structuring element we used either a sphere, when processing Set1, or a cylinder, when processing Set2. We remark that using a sphere on Set2 would produce very poor results due to the small number of pixels available along the z direction. On the other hand, our method using Directional ratio requires no *ad hoc* modifications for the two data sets.

The performance results of our method, denoted as 3D-DR, and the method based on the morphological opening operator, denoted as 3D-Mo are reported in Table 4.

Table 4: **Performance comparison.** Performance analysis of our 3D soma detection and extraction algorithms (3D-DR) and 3D-Mo, a method based on morphological operators. Results in the table are averages from image stacks of brain tissue (Set 1 = 3 stacks, 3 somas) and neuronal cultures (Set 2 = 3 stacks, 16 somas).

	3D-DR Sets 1+2	3D-Mo Sets 1+2	3D-DR Set 1	3D-Mo Set 1	3D-DR Set 2	3D-Mo Set 2
Detection rate	100%	100%	100%	100%	100%	100%
TPR (extraction)	0.91	0.89	0.93	0.95	0.89	0.83
FPR (extraction)	0.21	0.20	0.11	0.17	0.18	0.24
DC (extraction)	0.89	0.86	0.90	0.90	0.88	0.81
Comput. time	78 s	20 s	106 s	13 s	35 s	5 s

Table 4 shows that 3D-RD, our method based on Directional Ratio, provides overall a modest performance improvement with respect to 3D-Mo (DC: 0.89 vs. 0.86) at the expense of a higher computational cost (78 vs. 20 s). However, a closer examination of the results shows that 3D-DR exhibits a rather significant better performance with respect to 3D-Mo when the analysis is restricted to the image stacks of neuronal cultures (DC: 0.88 vs. 0.81). As observed above, confocal image stacks of neuronal cultures are more challenging to process since they contain a relatively small number of images, typically about 10-20 images, so that only 10-20 pixels is available along the z-direction. Unlike conventional morphological operators, the method based on Directional Ratio performs in this situation about as efficiently as for the other data. Even though, processing time is faster for 3D-Mo, computing time is very reasonable for 3D-DR.

4. Conclusion

We have introduced and applied a new algorithm for the automated detection and extraction of somas in *in vitro* 2D/3D fluorescent images of neurons. This method relies on a novel geometrical descriptor called Directional Ratio and is designed to process images where somas and other structures exist in the same fluorescent channel.

Our algorithm achieves highly accurate and ultra-fast soma detection by employing a family of multiscale orientable anisotropic filters that are implemented by separable convolution. Compared with state-of-the-art methods based on conventional morphological operators, our approach offers higher reliability (much fewer somas are missed or misidentified), much faster detection and significantly more accurate soma extraction. In addition, our algorithm is able to automatically separate contiguous soma in MIP image of neuronal cultures. With respect to an earlier application of the Directional Ratio, the new approach can process 2D images over 40 times faster and can be applied to process 3D image stacks, while this was virtually impossible before.

Even though our method is targeted to address challenges typically found in the analysis of confocal images of

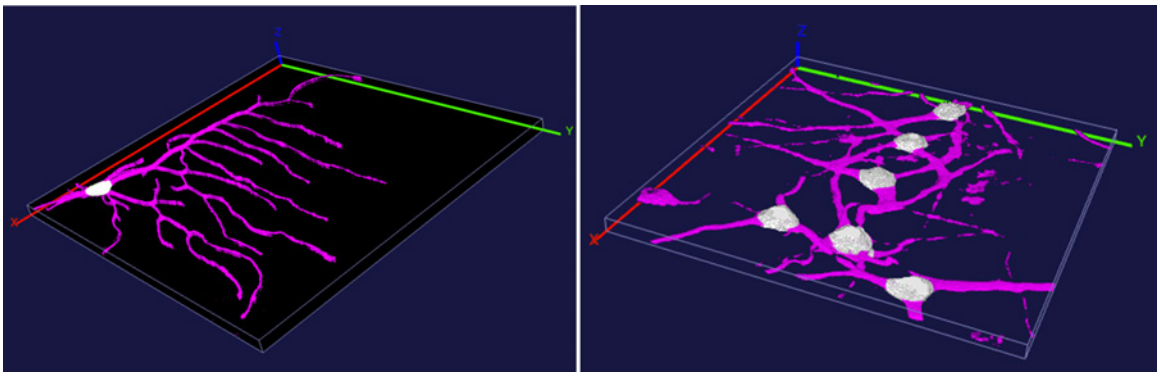

Figure 7: **3D soma extraction.** Soma detection and extraction using our algorithm based on Directional ratio and anisotropic Gaussian filters of a confocal image stack of a brain tissue (left) and a neuronal culture (right).

cultured neurons, its methodology also applies to bright field microscopy as well as to fluorescent images of brain tissue. In fact our set of numerical experiments includes 'simple' brain tissue images containing a single neuron. Dealing with more general fluorescent images of brain tissue poses potentially additional challenges as higher neuronal density and lower image contrast may become limiting factors for our algorithm. The extension of our method to these data will be explored in future studies.

Automated detection and segmentation of somas in fluorescent images of neurons is a critical tool not only for the identification and discrimination of neurons but also for the extraction of graph and connectivity properties in neuronal networks as somas provide ideal seed points for neuronal tracing algorithms [38]. Additionally, the methods based on directional filtering developed in this paper have potentially wider applicability for profiling morphological properties of neurons including alignment and spatial organization of neurites [39]. The ideas and results of this paper will facilitate the development of improved high-throughput platforms for the study of neuronal networks for HCS applications.

Acknowledgements

Authors thank one anonymous reviewer for useful suggestions about the use of automated scale selection. They also thank Dr. Laezza from the Department of Pharmacology & Toxicology of UTMB for useful discussions and for providing the confocal images used in the paper. DL acknowledges partial support of grant NSF-DMS 1320910.

References

[1] S. L. Senft, A brief history of neuronal reconstruction, Neuroinformatics 9 (2) (2011) 119–128. doi:10.1007/s12021-011-9107-0.

[2] R. Parekh, G. A. Ascoli, Neuronal morphology goes digital: a research hub for cellular and system neuroscience, Neuron 77 (6) (2013) 1017–1038. doi:10.1016/j.neuron.2013.03.008.

[3] D. E. Donohue, G. A. Ascoli, Automated reconstruction of neuronal morphology: An overview, Brain Research Reviews 67 (12) (2011) 94–102. doi:10.1016/j.brainresrev.2010.11.003.

[4] K. Svoboda, The past, present, and future of single neuron reconstruction, Neuroinformatics 9 (2011) 87–98. doi:10.1007/s12021-011-9097-y.

[5] K. A. Al-Kofahi, S. Lasek, D. H. Szarowski, C. J. Pace, G. Nagy, J. N. Turner, B. Roysam, Rapid automated three-dimensional tracing of neurons from confocal image stacks, IEEE Trans Inf Technol Biomed 6 (2) (2002) 171–187.

[6] Y. Al-Kofahi, N. Dowell-Mesfin, C. Pace, W. Shain, T. J. N., B. Roysam, Improved detection of branching points in algorithms for automated neuron tracing from 3D confocal images, Cytom Part A 73 (1) (2008) 36–43. doi:10.1002/cyto.a.20499.

[7] J. B. Pawley, Handbook of biological confocal microscopy, Springer, New York (N.Y.), 2006.

[8] C. M. Weaver, J. D. Pinezich, W. B. Lindquist, M. E. Vazquez, An algorithm for neurite outgrowth reconstruction., J. Neurosci. Methods 124 (2003) 197–205.

[9] K. El-Laithy, M. Knorr, J. Ks, M. Bogdan, Digital detection and analysis of branching and cell contacts in neural cell cultures, J. Neurosci. Methods 210 (2) (2012) 206–219. doi:10.1016/j.jneumeth.2012.07.007.

[10] W. He, T. A. Hamilton, A. R. Cohen, T. J. Holmes, C. Pace, D. H. Szarowski, J. N. Turner, B. Roysam, Automated three-dimensional tracing of neurons in confocal and brightfield images, Microsc. Microanal 9 (2003) 296–310.

[11] P. Vallotton, R. Lagerstrom, C. Sun, M. Buckley, D. Wang, et al., Automated analysis of neurite branching in cultured cortical neurons using hca-vision, Cytom. Part A 71 (10) (2007) 889–895. doi:10.1002/cyto.a.20462.

[12] S. K. Schmitz, J. J. Hjorth, R. M. Joemai, R. Wijntjes, S. Eijgenraam, P. de Bruijn, C. Georgiou, A. P. de Jong, A. van Ooyen, M. Verhage, L. N. Cornelisse, R. F. Toonen, W. Veldkamp, Automated analysis of neuronal morphology, synapse number and synaptic recruitment, J Neurosci Methods 195 (2) (2011) 185–193. doi:10.1016/j.jneumeth.2010.12.011.

[13] C. Yan, A. Li, B. Zhang, W. Ding, Q. Luo, H. Gong, Automated and accurate detection of soma location and surface morphologyin large-scale 3D neuron images, PLoS ONE 8 (4) (2013) 1–12. doi:10.1371/journal.pone.0062579.

[14] B. Ozcan, P. Negi, F. Laezza, M. Papadakis, D. Labate, Automated detection of soma location and morphology in neuronal network cultures, PloS One 10 (4). doi:10.1371/journal.pone.0121886.

[15] R. C. Gonzalez, R. E. Woods, S. L. Eddins, Digital Image Processing Using MATLAB, Prentice-Hall, Inc., Upper Saddle River, NJ, USA, 2003.

[16] D. L. Donoho, De-noising by soft-thresholding, IEEE Trans Info Theory 41 (3) (1995) 613–627.

[17] D. L. Donoho, J. M. Johnstone, Ideal spatial adaptation by wavelet shrinkage, Biometrika 81 (3) (1994) 425–455.

[18] D. Labate, F. Laezza, P. Negi, B. Ozcan, M. Papadakis, Efficient processing of fluorescence images using directional multiscale representations, Mathematical Modelling of Natural Phenomena 9 (5) (2014) 177–193. doi:10.1051/mmnp/20149512.

[19] F. Luisier, C. Vonesch, T. Blu, M. Unser, Fast haar-wavelet denoising of multidimensional fluorescence microscopy data, in: ISBI, 2009.

[20] B. Zhang, M.-J. Fadili, J.-L. Starck, Wavelets, ridgelets, and curvelets for poisson noise removal, IEEE Trans. Image Process 17 (2008) 1093–1108.

[21] D. Jiménez, D. Labate, I. Kakadiaris, M. Papadakis, Kakadiaris, Improved automatic centerline tracing for dendritic and axonal structures, Neuroinformatics 13 (2) (2015) 227–244. doi:10.1007/s12021-014-9256-z.

[22] D. Jiménez, D. Labate, M. Papadakis, Directional analysis of 3d tubular structures via isotropic well-localized atoms, Applied and Computational Harmonic Analysis 40 (3) (2016) 588 – 599. doi:10.1016/j.acha.2015.08.011.

[23] B. Ozcan, D. Labate, D. Jimenez, M. Papadakis, Directional and non-directional representations for the characterization of neuronal morphology, in: Wavelets XV (San Diego, CA, 2013), SPIE Proceedings, Vol. 8858, 2013, pp. 1050–1053.

[24] P. Perona, Steerable-scalable kernels for edge detection and junction analysis, Image Vision Comput. 10 (10) (1992) 663–672.

[25] G. R. Easley, D. Labate, W. Lim, Sparse directional image representations using the discrete shearlet transform, Appl. Comput. Harmon. Anal. 25 (2008) 25–46. doi:doi:10.1016/j.acha.2007.09.003.

[26] G. R. Easley, D. Labate, Image processing using shearlets, in: Shearlets: Multiscale Analysis for Multivariate Data, Appl. Numer. Harmon. Anal., Birkhäuser Boston, Boston, MA, 2012, pp. 283–325.

[27] J.-M. Geusebroek, A. Smeulders, J. van de Weijer, Fast anisotropic gauss filtering, IEEE Trans Image Process 12 (8) (2003) 938–943.

[28] C. H. Lampert, O. Wirjadi, An optimal nonorthogonal separation of the anisotropic gaussian convolution filter, IEEE Trans Image Process 15 (11) (2006) 3501–3513.

[29] S. Osher, R. P. Fedkiw, Level set methods and dynamic implicit surfaces, Applied mathematical science, Springer, New York, N.Y., 2003.

[30] J. A. Sethian, Level Set Methods and Fast Marching Methods., 2nd Edition, Cambridge University Press, 1999.

[31] T. Deschamps, L. D. Cohen, Fast extraction of minimal paths in 3d images and applications to virtual endoscopy, Medical image analysis 5 (4) (2001) 281–299.

[32] A. S. Shavkunov, N. C. Wildburger, M. N. Nenov, T. F. James, T. P. Buzhdygan, N. I. Panova-Elektronova, T. A. Green, R. L. Veselenak, N. Bourne, F. Laezza, The fibroblast growth factor 14voltage-gated sodium channel complex is a new target of glycogen synthase kinase 3 (GSK3), J Biol. Chem. 288 (27) (2013) 19370–85. doi:10.1074/jbc.M112.445924.

[33] D. G. Altman, J. M. Bland, Diagnostic tests. 1: Sensitivity and specificity., BMJ 308 (6943) (1994) 15–52.

[34] R. Dolmetsch, D. H. Geschwind, The human brain in a dish: The promise of iPSC-derived neurons, Cell 145 (6) (2011) 831–834.

[35] T. J. F. Nieland, D. J. Logan, J. Saulnier, D. Lam, C. Johnson, D. E. Root, A. E. Carpenter, B. L. Sabatini, High content image analysis identifies novel regulators of synaptogenesis in a high-throughput rnai screen of primary neurons, PLoS ONE 9 (3). doi:dx.doi.org/10.1371/journal.pone.0091744.

[36] K. Sharma, S.-Y. Choi, Y. Zhang, T. J. Nieland, S. Long, M. Li, R. L. Huganir, High-throughput genetic screen for synaptogenic factors: Identification of LRP6 as critical for excitatory synapse development, Cell Reports 5 (5) (2013) 1330 – 1341. doi:10.1016/j.celrep.2013.11.008.

[37] T. Lindeberg, Feature detection with automatic scale selection, International Journal of Computer Vision 30 (2) (1998) 79–116.

[38] E. Meijering, Neuron tracing in perspective, Cytom Part A 77A (7) (2010) 693–704. doi:10.1002/cyto.a.20895.

[39] P. Singh, P. Negi, F. Laezza, M. Papadakis, D. Labate, Multiscale analysis of neurite orientation and spatial organization in neuronal images, Neuroinformatics (2016) 1–13doi:10.1007/s12021-016-9306-9.